เอกสารอ้างอิง

1. Chou, H., et al., *Langmuir-Blodgett Films of Amphiphilic Push-Pull Porphyrins.* J. Phys. Chem.,·1994. 98: p. 383-385.
2. Yamada, S., et al., *Second-Order Nonlinear Optical Properties of Amphiphilic Porphyrins in Langmuir-Blodgett Monolayer Assemblies.* J. Photochem. Photobio. A, 1995. 87: p. 115-119.
3. Qian, X., et al., *Molecular Packing in LB Films of a New Porphyrin Investigated by Atomic Force Microscopy.* Thin Solid Films, 1996. 284-285: p. 432-435.
4. Qian, D.-J., C. Nakamura, and J. Miyake, *Spectroscopic Studies of the Multiporphyrin Arrays at the Air–Water Interface and in Langmuir–Blodgett Films.* Thin Solid Films, 2001. 397: p. 266-275.
5. Paolesse, R., et al., *Langmuir–Blodgett Films of a Modified Tetraphenylporphyrin.* Mat. Sci. Eng. C, 2002. 22: p. 219-225.
6. Koo, J.-R., et al., *Electrical Properties of Porphyrin-Based Switching Devices.* Thin Solid Films, 2003. 438-439: p. 123-127.
7. Boguta, A., et al., *Characterization of Interfacial Effects in Organic Macrocycles Langmuir and Langmuir–Blodgett Layers Studied by Surface Potential and FT–IR Spectroscopy Examination.* Mat. Sci. Eng. B, 2004. 113: p. 99-105.
8. Zhou, Y., et al., *Observation of Co-Existence of "face-on" and "edge-on" Stacking Styles in a Porphyrin Monolayer.* Chem. Phys. Lett., 2005. 403: p. 140-145.
9. Tronin, A., et al., *Determination of the Porphyrin Orientation Distribution in Langmuir Monolayers by Polarized Epifluorescence.* Langmuir, 2000. 16: p. 9878-9886.
10. Imahori, H., et al., *Concentration Effects of Porphyrin Monolayers on the Structure and Photoelectrochemical Properties of Mixed Self-Assembled Monolayers of Porphyrin and Alkanethiol on Gold Electrodes.* Langmuir, 2001. 17: p. 4925-4931.
11. Pedrosa, J.M., et al., *Influence of Molecular Organization of Asymmetrically Substituted Porphyrins on Their Response to NO2 Gas.* Langmuir, 2002. 18: p. 7594-7601.
12. Lamoen, D. and M. Parrinello, *Geometry and Electronic Structure of Porphyrins and Porphyrazines.* Chem. Phys. Lett., 1996. 248: p. 309-315.
13. Rovira, C., P. Ballone, and M. Parrinello, *A Density Functional Study of Iron-Porphyrin Complexes.* Chem. Phys. Lett., 1997. 271: p. 247-250.

14. Oliveira, K.M.T. and M. Trsic, *Comparative Theoretical Study of the Electronic Structures and Electronic Spectra of Fe^{2+}-, Fe^{3+}-Porphyrin and Free Base Porphyrin.* J. Mol. Struct. (Theochem), 2001. 539: p. 107-117.

15. Baerends, E.J., et al., *A DFT/TDDFT Interpretation of the Ground and Excited States of Porphyrin and Porphyrazine Complexes.* Coord. Chem. Rev., 2002. 230: p. 5-27.

16. Richardson, T.H., et al., *Taking Advantage of Optical and Electrical Properties of Organic Molecules for Gas Sensing Applications.* Thin Solid Films, 2001. 393: p. 259-266.

17. Spadavecchia, J., et al., *Spin-Coated Thin Films of Metal Porphyrin–Phthalocyanine Blend for an Optochemical Sensor of Alcohol Vapours.* Sens. Actuators B, 2004. 100: p. 88-93.

18. Petty, M.C., *Langmuir-Blodgett Films: An Introduction.* 1 ed. 1996, Cambridge: Cambridge University Press.

19. Liu, H.-G., et al., *Monolayer Studies on an Acetic Acid Substituted Porphyrin and Its Complexes with Aliphatic Amines or Quaternary Ammonium Salts at the Air-Liquid Interface.* Langmuir, 2000. 16: p. 5079-5085.

20. Gregory, B.W., et al., *Two-Dimensional Crystallization of Phthalocyanine Pigments at the Air/Water Interface.* J. Phys. Chem. B, 1999. 103: p. 502-508.

21. Bocker, J., et al., *Molecular Dynamics Simulation of a n-Hexadecyltrlmethylammonlum Chloride Monolayer.* J. Phys. Chem., 1992. 96(24): p. 9915-9922.

22. Ahlstrom, P. and H.J.C. Berendsen, *A Molecular Dynamics Study of Lecithin Monolayers.* J. Phys. Chem., 1993. 97: p. 13691-13702.

23. Karaborni, S., *Molecular Dynamics Simulations of Long-Chain Amphiphilic Molecules in Langmuir Monolayers.* Langmuir, 1993. 9: p. 1334-1343.

24. Siepmann, J.I., S. Karabomi, and M.L. Klein, *Monte Carlo Simulation of the Liquid-Vapor Coexistence in a Langmuir Monolayer of Pentadecanoic Acid.* J. Phys. Chem., 1994. 98: p. 6675-6678.

25. Tarek, M., D.J. Tobias, and M.L. Klein, *Molecular Dynamics Simulation of Tetradecyltrimethylamonium Bromide Monolayers at the Air/Water Interface.* J. Phys. Chem. A, 1995. 99: p. 1393-1402.

26. Dominguez, H., A.M. Smondyrev, and M.L. Berkowitz, *Computer Simulations of Phosphatidylcholine Monolayers at Air/Water and CCl_4/Water Interfaces.* J. Phys. Chem. B, 1999. 103: p. 9582-9588.

27. Kuhn, H. and H. Rehage, *Molecular Dynamics Computer Simulations of Surfactant Monolayers: Monododecyl Pentaethylene Glycol at the Surface between Air and Water.* J. Phys. Chem. B, 1999. 103: p. 8493-8501.

28. Okamura, E., N. Fukushima, and S. Hayashi, *Molecular Dynamics Simulation of the Vibrational Spectra of Stearic Acid Monolayers at the Air/Water Interface.* Langmuir, 1999. 15: p. 3589-3594.

29. Rovillard, S., et al., *Monolayer Organization Modeling Using Molecular Dynamics.* Langmuir, 1999. 15: p. 2749-2754.

30. Schmid, F., C. Stadler, and H. Lange, *Theoretical Modeling of Langmuir Monolayers.* Colloid Surface A, 1999. 149: p. 301-306.

31. Dominguez, H. and M.L. Berkowitz, *Computer Simulations of Sodium Dodecyl Sulfate at Liquid/Liquid and Liquid/Vapor Interfaces.* J. Phys. Chem. B, 2000. 104: p. 5302-5308.

32. Kuhn, H. and H. Rehage, *Molecular Orientation of Monododecylpentaethylene Glycol at Water/Air and Water/Oil Interfaces. A Molecular Dynamics Computer Simulation Study.* Colloid Polym Sci, 2000. 278: p. 114-118.

33. Shelley, M.Y., M. Sprik, and J.C. Shelley, *Pattern Formation in a Self-Assembled Soap Monolayer on the Surface of Water: A Computer Simulation Study.* Langmuir, 2000. 16: p. 626-630.

34. Opps, S.B., et al., *Monte Carlo Studies of Model Langmuir Monolayers.* Phys. Rev. E, 2001. 63: p. 041602-12.

35. Tomassone, M.S., et al., *Molecular Dynamics Simulation of Gaseous–Liquid Phase Transitions of Soluble and Insoluble Surfactants at a Fluid Interface.* J. Chem. Phys., 2001. 115(18): p. 8634-8642.

36. Bandyopadhyay, S. and J. Chanda, *Monolayer of Monododecyl Diethylene Glycol Surfactants Adsorbed at the Air/Water Interface: A Molecular Dynamics Study.* Langmuir, 2003. 19: p. 10443-10448.

37. Nicolas, J.P., *Molecular Dynamics Simulation of Surfactin Molecules at the Water-Hexane Interface.* Biophys. J., 2003. 85: p. 1377-1391.

38. Borodin, A. and M. Kiselev, *Structure of the Porphyrazine Monolayer at the Air–Water Interface: Computer Simulation.* Pure Appl. Chem., 2004. 76(1): p. 197-202.

39. Dominguez, H., *Computer Simulation Studies of Surfactant Monolayer Mixtures at the Water/Oil Interface: Charge Distribution Effects.* J. Colloid Interface Sci., 2004. 274: p. 665-672.

40. Rosa, M.L., et al., *A Molecular Dynamics Study of Monolayers of Nonionic Poly(ethylene oxide) Based Surfactants.* Langmuir, 2004. 20: p. 1375-1385.

41. Chanda, J., S. Chakraborty, and S. Bandyopadhyay, *Monolayer of Aerosol-OT Surfactants Adsorbed at the Air/Water Interface: An Atomistic Computer Simulation Study.* J. Phys. Chem. B, 2005. 109: p. 471-479.

42. Ivanova, A., et al., *Hydrophilic Interactions between Organic and Water Molecules as Models for Monolayers at the Gas/Water Interface.* J. Phys. Chem. A, 2005. 109: p. 1692-1702.

43. Kim, H.-Y. and K.A. Fichthorn, *Molecular Dynamics Simulation of Amphiphilic Dimers at a Liquid-Vapor Interface.* J. Chem. Phys., 2005. 122: p. 034704-7.

44. Knecht, V., et al., *Simulation Studies of Pore and Domain Formation in a Phospholipid Monolayer.* J. Chem. Phys., 2005. 122: p. 024704-9.

45. Moura, A.F.d. and M. Trsic, *Molecular Dynamics Simulation of a Perylene-Derivative Langmuir Film.* J. Phys. Chem. B, 2005. 109: p. 4032-4041.

46. Valkova, L., et al., *Three-Dimensional Structure of the Copper Porphyrazine Layers at the Air–Water Interface.* Thin Solid Films, 2001. 401: p. 267-272.

47. Valkova, L., et al., *Structure of Monolayers of Copper Tetra-(3-nitro-5-tert-butyl)-phthalocyanine at the Air-Water Interface.* Langmuir, 2001. 17: p. 3639-3642.

48. Hunter, C.A. and J.K.M. Sanders, *The Nature of p-p Interactions.* J. Am. Chem. Soc., 1990. 112: p. 5525-5534.

49. Biesaga, M., K. Pyrzynska, and M. Trojanowicz, *Porphyrins in Analytical Chemistry. A Review.* Talanta, 2000. 51: p. 209-224.

50. Marques, H.M. and K.L. Brown, *Molecular Mechanics and Molecular Dynamics Simulations of Porphyrins, Metalloporphyrins, Heme Proteins and Cobalt Corrinoids.* Coord. Chem. Rev., 2002. 225: p. 123-158.

ภาคผนวก

1. บทความวิชาการที่ได้รับการตีพิมพ์ในวารสารนานาชาติ
2. บทคัดย่อในการนำเสนอผลงานประชุมวิชาการ "ประชุมนักวิจัยรุ่นใหม่ พบ เมธีวิจัยอาวุโส สกว. ครั้งที่ 8 และครั้งที่ 9"

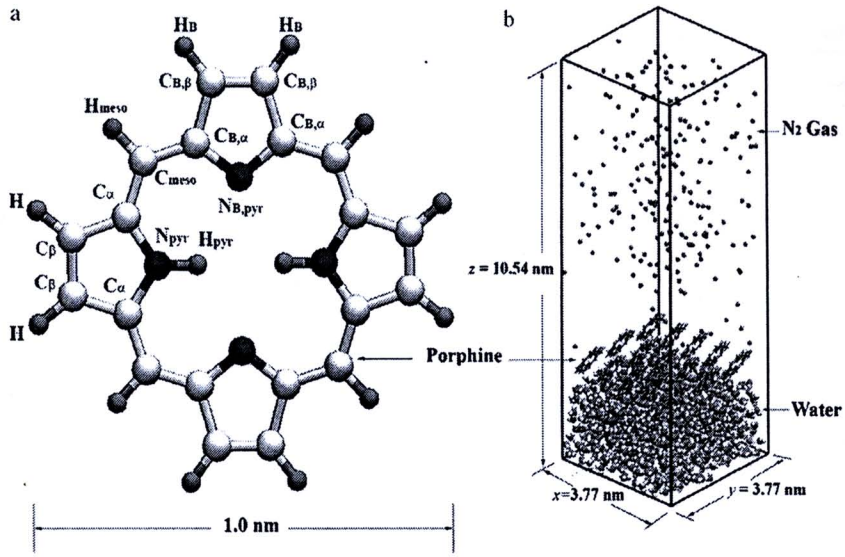

Fig. 1. (a) Porphine (PH_2) geometry and definition of its atom types: nitrogen (blue), carbon (white) and hydrogen (gray) and (b) a schematic representation of the initial configuration for the PH_2 monolayer in a rectangular box in which the z-axis is chosen to be perpendicular to the interface. (For interpretation of the references to color in this figure caption, the reader is referred to the web version of the article.)

ordered as concentration increase. For comparison, it is interesting to investigate in the same manner for the porphine molecule that has a similar structure with different donor atoms at the *meso* positions. Therefore, in this study, five different surface concentrations of PH_2 molecules, covering a full range of the π–A isotherm, were investigated using molecular dynamics computer simulation technique.

2. Materials and methods

2.1. Potential function models

The potential model describing intermolecular interactions of all molecules in monolayer model system is based on the pair-wise additive approximation, which is the sum of the Lennard–Jones and Coulomb interactions as given in Eq. (1),

$$U_{pair} = \sum_i \sum_j \left\{ 4\varepsilon_{ij} \left[\left(\frac{\sigma_{ij}}{r_{ij}} \right)^{12} - \left(\frac{\sigma_{ij}}{r_{ij}} \right)^{6} \right] + \frac{q_i q_j}{r_{ij}} \right\} \quad (1)$$

Here, r_{ij} is the distance between atom type i and j, q is the atomic charge, and σ and ε are the Lennard–Jones parameters (see details in Table 1). The cross interactions (i.e., Lennard–Jones term) between the two different atom types were obtained via the Lorentz–Berthelot combination rule. The Lennard–Jones parameters for water, PH_2 and nitrogen molecules were taken from the OPLS force field [28]. Molecular geometry and charge distribution of PH_2 molecule were obtained from quantum chemical calculations. The density functional theory method with the 6-31G** basis set (B3LYP/6-31G**) was employed. This method has been successfully applied for reproducing physical properties and electronic structures of the free base porphyrin molecule [19,29] and shows good agreement with the results obtained by Parrinello [23] and Kozlowski [22]. A charge distribution of the PH_2 molecule was obtained via Mulliken population analysis. The SPC model [30] was employed to describe water–water interactions and the united atom description was applied to the nitrogen molecule. Both PH_2 and water molecules were kept as rigid bodies throughout the simulations. The molecular geometries were constrained via the SHAKE algorithm [31]. The Lennard–Jones parameters and atomic charges for each atomic type in this model are summarized in Table 1.

2.2. Simulation details

Molecular dynamics simulations were performed for the PH_2 monolayer at the water–nitrogen gas interface having different surface concentrations which corresponds to the numbers of 10, 15, 20, 25, and 30 PH_2 molecules per an area of 3.77 nm × 3.77 nm, respectively (as denoted by systems A–E). Such surface concentrations cover a full range of the experimental π–A isotherm [16]. The simulations were carried out in the periodic rectangular box having a volume of 3.77 nm × 3.77 nm × 10.54 nm, which contained 864 water and 216 nitrogen molecules. The initial configurations of the PH_2 monolayers were generated in a regular pattern and then inserted at the water–gas interface system which was taken from previous our work [20]. Schematic representation of the PH_2 monolayer at the water–gas interface is depicted in Fig. 1(b) in which the z-axis was chosen to be perpendicular to the interface. It is important to note that a sufficiently large size of the simulated box in the z-axis (more than 100 Å) was necessary in order to avoid artificial interactions between particles in the central box and its replica [32]. All five system models were simulated at a canonical ensemble which a number of atoms (N), volume (V) and temperature (T) were kept constant. A constant temperature of 300 K was maintained by using the Berendsen–thermostat [33] with a coupling constant of 0.1 ps. Water, PH_2 and N_2 molecules were coupled individually to the heat bath. The equations of motion were integrated using a leapfrog algorithm with a time step of 2 fs. The systems were equilibrated for a period of 5 ns, followed by a 2 ns simulation for data collection. During the entire simulations, periodic boundary conditions were applied in all three spatial directions. The electrostatic interactions were calculated using the Fast Particle Mesh Ewald method (PME) method [34]. Fourth order (cubic) interpolation was used with a real space cutoff of 1.0 nm and a grid spacing of 0.12 nm. Van der Waals interactions were cutoff after a distance of 1.5 nm. These simulations were performed using the Gromacs package version 3.2.1 [35,36]. Molecular visualization was carried out by using the VMD program [37].

Please cite this article in press as: S. Krongsuk, T. Kerdcharoen, Effects of surface concentration on the porphine monolayers: Molecular simulations at the nanoscale water–gas interface, Appl. Surf. Sci. (2011), doi:10.1016/j.apsusc.2011.02.058

Table 1
Definition of atom types, atomic charges and Lennard–Jones parameters for water (H_2O), porphine (PH_2), and nitrogen (N_2) molecules, respectively.

Molecule	Atom type	Charge	ε (kJ mol^{-1})	σ (nm)
H_2O	O	−0.820	0.6500	0.316
H_2O	H	0.410	0.000	0.000
PH_2	C_{meso}	−0.278	0.2929	0.350
PH_2	N_{pyr}	−0.673	0.7115	0.325
PH_2	C_α	−0.192	0.2929	0.355
PH_2	C_β	0.399	0.2929	0.355
PH_2	H	0.131	0.0000	0.000
PH_2	$N_{B,pyr}$	−0.760	0.7115	0.325
PH_2	$C_{B,\alpha}$	−0.179	0.2929	0.355
PH_2	$C_{B,\beta}$	0.347	0.2929	0.355
PH_2	H_B	0.145	0.0000	0.000
PH_2	H_{pyr}	0.415	0.1256	0.242
PH_2	H_{meso}	0.137	0.0000	0.000
N_2	N_2	0.000	0.5937	0.379

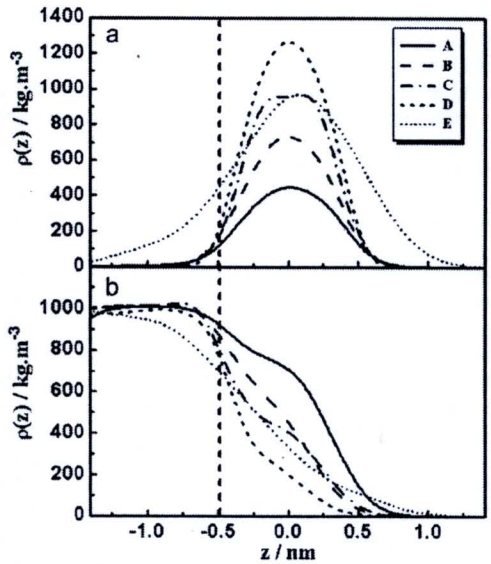

Fig. 2. Density profiles of (a) PH_2 and (b) water molecules as a function of z-coordinate for five simulated systems. The vertical dash line indicates the interface boundary (see definition in Section 3.1).

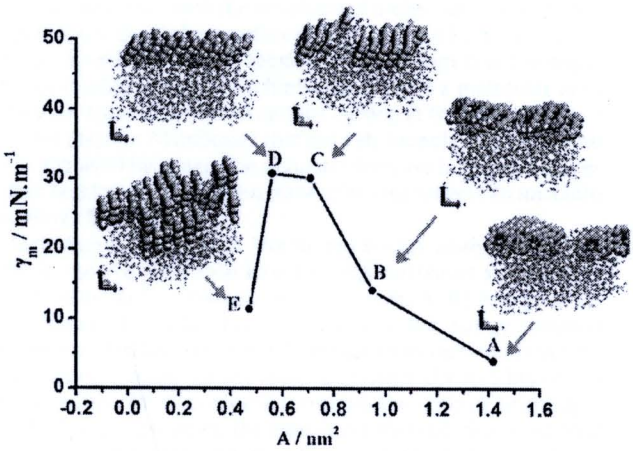

Fig. 3. Monolayer surface tension (γ_m) of the PH_2 monolayers as a function of molecular area (A) for the five surface concentrations. Insets of Fig. 3 correspond to gaseous (system A), expanded (system B), condensed (systems C and D), and collapsed (system E) phases, respectively.

3. Results and discussion

3.1. Density profiles

To characterize the interfacial behaviors of the PH_2 monolayer, the density profiles of PH_2 and water molecules as a function of z-coordinates were calculated. To identify the interface position (z_i) between water and PH_2 molecules, the average z-positions (z_0) of PH_2 molecules were calculated via Eq. (2) and then $z_i = z_0 - 0.5$:

$$z_0 = \frac{\int z.\rho(z)dz}{\int \rho(z)dz} \quad (2)$$

Here, $\rho(z)$ is the mass density of PH_2 molecules and the numerical value of 0.5 is estimated from a half diameter of the PH_2 molecule. For systematic comparison, it is convenient to shift the averaged position, z_0, to be zero. The PH_2 and water densities are displayed in Fig. 2(a) and (b), respectively. As seen in Fig. 2(a), adding more PH_2 molecules onto the gas–water interface leads to increasing peak height. However, it appears that the peak height is saturated at the surface density of 25 molecules per an area of 3.77 nm × 3.77 nm (system D) and thus addition of the PH_2 molecules beyond this surface density results in a widening peak width.

The PH_2 density curves as they appear in Fig. 2(a) can be classified into four groups, corresponding to the gaseous (system A), expanded (systems B), condensed (systems C and D), and collapsed (system E) phases of the PH_2 monolayers, respectively, according to a full range of the π–A isotherm plot (see detailed discussion in Section 3.2). For the gaseous phase (system A), it is clearly seen that the PH_2 probability distribution is low and quite broad. Each PH_2 molecule in the monolayer has a sufficiently large free area (molecular area ~ 1.42 nm^2). Under such circumstances, water molecules are likely to fill up the empty space as seen in Fig. 2(b) where the water density profile is still prominent beyond the interface position ($z_i = -0.5$ nm). The density profile of water is significantly reduced for the expanded (system B), condensed (system C and D), and collapsed (system E) phases. A clear picture of these results can be more conceivably presented by simulation snapshots as shown in the inset of Fig. 3.

In Fig. 2(a), the density peak of PH_2 molecules increases as more PH_2 molecules are added into the monolayer (systems A–D). However, the density curve of system E becomes lower and broad indicating that the monolayer in this system has collapsed. It can be explained that as the PH_2 molecules are too closely packed, their molecular arrangements are re-adjusted to minimize the repulsive interaction. Consequently, some PH_2 molecules are pushed out from the initial monolayer into the water and gas phases. Hunter and Sanders [38] reported that the optimized geometry of porphine–porphine dimer is observed in such a way that the pyrrole ring of one porphine align directly above the π-cavity at the

Please cite this article in press as: S. Krongsuk, T. Kerdcharoen, Effects of surface concentration on the porphine monolayers: Molecular simulations at the nanoscale water–gas interface, Appl. Surf. Sci. (2011), doi:10.1016/j.apsusc.2011.02.058

Table 2
Molecular area (A), a number of hydrogen bonds (n_{HB}), interaction energies of the PH_2–PH_2 and the PH_2–water systems, and an average distance between the center of mass of the nearest neighbors PH_2 molecules (d) in five surface concentrations.

System	A (nm^2)	n_{HB}	Interaction energy (kJ/mol)		d (nm)
			PH_2–PH_2	PH_2–water	
A	1.42	1.48 ± 0.02	−184.77 ± 9.02	−195.82 ± 7.83	0.447 ± 0.013
B	0.95	0.78 ± 0.10	−213.32 ± 10.83	−127.75 ± 5.39	0.442 ± 0.013
C	0.71	0.56 ± 0.07	−245.74 ± 9.85	−107.05 ± 3.85	0.450 ± 0.013
D	0.56	0.34 ± 0.05	−305.46 ± 10.78	−75.25 ± 3.18	0.423 ± 0.011
E	0.47	0.47 ± 0.06	−249.22 ± 11.07	−100.07 ± 3.76	0.446 ± 0.014

center of the other. This arrangement yields optimal π–π interactions. It is also seen that an average distance (d) between the nearest neighbors of the PH_2 molecules given in Table 2 is nearly the same for all five systems. This value (~0.4 nm) is larger than an optimal distance of the PH_2 dimer system (0.34 nm). It causes water contribution to the PH_2–PH_2 interactions. A previous LB experiment on copper porphyrazine (CuPz) [16] showed that the CuPz monolayer formation starts to be observed at a molecular area of 1.25 nm^2 for the lowest initial concentration. This study also reported the limiting molecular area for compression of such monolayers ranging 0.40–0.55 nm^2, depending on the initial surface concentrations. Qian et al. [6] prepared a monolayer film of tetrapyridylporphyrin (TPyP) on a water subphase with a molecular area of 0.65 nm^2. Our results are in agreement with the experimental observations as will be discussed further.

In Fig. 2(b), the water density profiles for all five systems are plotted according to two regions; one region lying below the interface position and another one above it. Below the interface boundary, the water densities for all systems, excluding system E, simply fluctuate around the bulk density value. Inside the interface region, the water densities for all systems rapidly decrease from the bulk density value as increasing number of PH_2 molecules are added into the interface. It is seen from Fig. 2 that an increasing number of PH_2 molecules clearly affects the water density profile at the interface. For system A, the water density at the interfacial region is the highest because there is the lowest number of PH_2 molecules there. In such a case, all PH_2 molecules in the system are easily dissolved by water molecules. The water density beyond the interface position is significantly decreased and approaches zero about 1.0 nm from the interface position. Some water molecules associated with the hydration structure of the PH_2 molecules are assumed to be the "guest"-water molecules, which are preferentially oriented in such a way to maximize the hydrogen bonding with the PH_2 molecules [19]. It was also observed that the number of the guest-water molecules in the hydration shells decreases as the surface concentration increases [16].

3.2. Monolayer surface tension

The surface tension, γ_s, was calculated from the diagonal components of the pressure tensor as follows:

$$\gamma_s = \left(P_{zz} - \left(\frac{P_{xx} + P_{yy}}{2}\right)\right) L_z \quad (3)$$

where L_z is the z-component of the box size, P_{zz} is the normal pressure and $(P_{xx} + P_{yy})/2$ is the lateral pressure. In this simulation there are two interfaces that have a surface tension. These are the PH_2/water interface (monolayer) and the water/gas interface at the bottom of the water layer. Hence,

$$\gamma_s = \gamma_m + \gamma_{wg} \quad (4)$$

where γ_m is the monolayer surface tension and γ_{wg} is the surface tension at the water/gas interface. In order to calculate γ_m it was first necessary to determine γ_{wg}. MD simulation was performed on a water layer with the PH_2 molecules removed. The water simulation was run for 3 ns using the same simulation parameters as had been used for the PH_2 simulations. The monolayer surface tension as a function of the area per PH_2 molecules is given in Fig. 3. It is clearly seen that the monolayer surface tension of the PH_2 molecules increases with the reduction of molecular area and suddenly drops at the highest surface density (system E). It is also seen that the monolayer surface tension of the system D is the highest. This implies that the film formation at such a molecular area is the most stable. The lowest surface tension at the largest molecular area (system A) indicates that the PH_2 monolayer film can be easily dissolved by water. The dramatic decrease in the monolayer surface tension at the smallest molecular area reflects an unstable monolayer film.

According to an average interaction energy analysis given in Table 2, the PH_2–PH_2 interaction energy decreases significantly as increasing surface concentration (systems A–D) and goes up at the system E, but the PH_2–water interaction energy shows a reverse direction This result indicates that an increment of the PH_2 molecules on a water surface leads to enhance the stability of the PH_2 monolayer formation until it reaches the optimal point (system D). Beyond this point, the monolayer film stability is reduced because some PH_2 molecules start to move out from the monolayer (i.e., some diffuse into the water bulk and into the gas phase). Consequently, the collapsed phase of the PH_2 monolayer at the molecular area results. Capan et al. [13] reported three existent monolayer phases of the free base porphyrin including gaseous, expanded, and condensed phases. Our result not only gives good agreement with the experimental data [16], but also exhibits a clear picture of phase transfer of the PH_2 monolayers as depicted in the insets of Fig. 3.

3.3. Hydrogen bonding

The π–π interaction concept usually proposed as an explanation for the stability of the phtalocyanines packing [8] may not be used alone as the major role for PH_2 stability [19]. Thus, water–PH_2 interaction through hydrogen bonding was found to play another important role in keeping the whole balance of the system. As clearly seen in Table 2, the interaction energy between the PH_2 and water molecules reduces as the number of PH_2 molecules increases excluding the highest surface concentration. This suggests that the hydrogen bonding is less contribution to the monolayer film stability at the higher surface concentrations. Characteristics of hydrogen bonding between water and PH_2 molecules can be investigated by means of hydrogen bond analysis. To determine the existence of hydrogen bond, a geometrical criterion for donor and acceptor atoms is used (i.e., $r \leq 0.35$ nm, $\alpha \leq 60°$). In our models, N atoms of PH_2 and O atoms of water are considered as acceptors and donors, respectively. The average values of hydrogen bonds, n_{HB}, calculated as a function of molecular area (A) are given in Fig. 4. A number of hydrogen bond is reduced with decreasing molecular area. For the higher surface concentrations (systems C–E) molecular packing of the PH_2 molecules force them to be tilted enough that hydrogen bonding between N atoms of PH_2 and bulk water is too difficult. Fur-

Please cite this article in press as: S. Krongsuk, T. Kerdcharoen, Effects of surface concentration on the porphine monolayers: Molecular simulations at the nanoscale water–gas interface, Appl. Surf. Sci. (2011), doi:10.1016/j.apsusc.2011.02.058

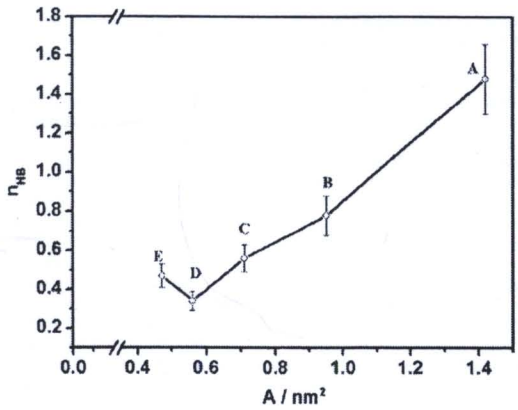

Fig. 4. Average hydrogen bond number (n_{HB}) as a function of molecular area (A) for the five different surface concentrations.

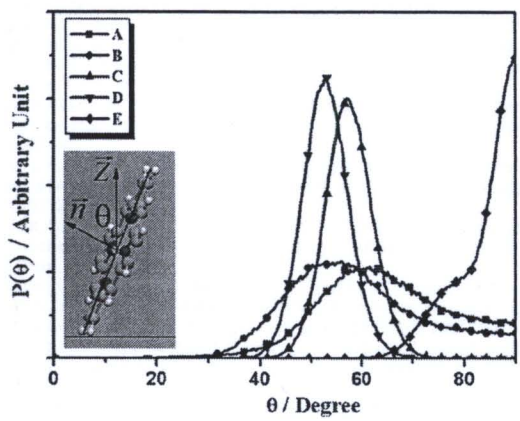

Fig. 5. Distributions of tilt angle, $P(\theta)$, of the PH_2 molecules on the water–gas interface for the five different surface concentrations.

thermore, an increment in PH_2 surface concentration also removes guest-water molecules that can form additional hydrogen bonds. These characteristics are similarly observed in our previous study in which a porphyrazine monolayer at the water–gas interface was simulated [20]. In that case, hydrogen bonds contribute to the film stability to a larger extent.

Summation over all hydrogen bonds leads to a relatively complicated dependence of hydrogen bonding on surface concentration. Fig. 4 shows the relation between average number of hydrogen bonds and molecular area. This plot reveals that an increment in surface concentration (from systems A to D) causes significant decline in the hydrogen bond number as a result of the reduction in guest-water molecules as well as a steeper tilted orientation of PH_2 over the water surface. However, further increase in surface density from the systems D to E surprisingly brings the hydrogen bond number up again. This results suggest that hydrogen bonding plays an important role in the stability of the film formation, apart from the usually believed $\pi-\pi$ interactions [38].

3.4. Molecular orientation

Molecular orientation of the PH_2 molecules can be extracted from a probability distribution of a molecular tilt angle, $P(\theta)$. The tilt angle, θ, is defined as an angle between the normal vector perpendicular to the molecular plane ($\vec{n}$) and the vector parallel to the z-axis ($\vec{z}$) as shown in an inset of Fig. 5. This probability distribution is calculated for all five systems and plotted in Fig. 5.

For the two lower surface concentrations (systems A and B), the tilt angle distributions of PH_2 molecules are quite broad, which indicates that PH_2 molecules are preferentially oriented with tilt angles ranging from 30° to 90°. It is clear that the PH_2 molecules in the lower surface concentrations (systems A and B) have more possibility for molecular orientations, which would not be possible for the other systems (C–E). In the condensed phase (systems C and D) the PH_2 molecules are closely packed. The probability distribution of the tilt angle shows a sharp peak at the angles of 57° and 53° for the systems C and D, respectively. These angles are assumed to be the β-structure (47°) as observed in the CuPz monolayer film at the lower surface concentration [16]. For the highest concentration (system E), the tilt angles start to be observed from 60° up to 90°. The maximum peak centered at 90° indicates that the PH_2 molecules preferentially orient their molecular plane perpendicular to the interface. Valkova et al. [8,16] found that the molecular orientation of copper phthalocyanine (CuPc) monolayers on water surface can be formed in one of the three types of phase state including the β (45°), α (65°), and x (90°) structure, depending on initial experimental conditions. They reported that the β-structure of the layers is more favored in gaseous phase (lower concentration), while the β- and α-forms are observed in the condensed phase. For higher concentration the x-form is dominant. Our results exhibit that the PH_2 monolayers are favored to be the β-structure for all systems except the highest surface concentration (system E) which it is favored to be the x-structure.

4. Summary

In this study we have shown that molecular dynamics simulations using a simplified model for the PH_2 monolayer at the water–gas interface can clarify the phase transforms and monolayer structure. In particular, these simulations exhibit that the phase transfer of the PH_2 monolayer i.e., from the gaseous to the expanded phase, from the expanded to the condensed phase, and the condensed to the collapsed phase can be observed with increasing surface concentrations. Such results are in good agreement with the π–A isotherm curves of CuPz monolayer obtained from experiment [16]. In addition, we have found that the formation of the PH_2 monolayer film is strongly influenced by changing the number of PH_2 molecules at the water surface as summarized in the following conclusions. (i) The PH_2 molecules are closely packed and regularly formed at increasing surface concentrations. (ii) A reduction of the guest-water molecules at the interface due to increasing the PH_2 molecules not only causes better formation of monolayer film, but also improves the film stability. We believe that the hydrogen bonding plays a crucial role apart from the $\pi-\pi$ interactions. (iii) Finally, for the PH_2 monolayers, the β-structure is the more favored of all the monolayer phases, except the collapsed one that shows the x-structure.

Acknowledgements

This work was financially supported by a Basic Research Grant from the Thailand Research Fund. A career development fellowship from the Thailand Research Fund in cooperation with the Commission on Higher Education given to S.K. (MRG5080218) is acknowledged. The authors thank Dr. Jeff Johns for proofreading of the manuscript.

References

[1] H. Chou, C.-T. Chen, K.F. Stork, P.W. Bob, K.S. Suslick, Langmuir–Blodgett films of amphiphilic push–pull porphyrins, J. Phys. Chem. 98 (1994) 383–385.
[2] S. Yamada, K. Kuwata, H. Yonemura, T. Matsuo, Second-order nonlinear optical properties of amphiphilic porphyrins in Langmuir–Blodgett monolayer assemblies, J. Photochem. Photobiol. A: Chem. 87 (1995) 115–119.

Please cite this article in press as: S. Krongsuk, T. Kerdcharoen, Effects of surface concentration on the porphine monolayers: Molecular simulations at the nanoscale water–gas interface, Appl. Surf. Sci. (2011), doi:10.1016/j.apsusc.2011.02.058

[3] X. Qian, Z. Tai, X. Sun, S. Xiao, H. Wu, Z. Lu, Y. Wei, Molecular packing in LB films of a new porphyrin investigated by atomic force microscopy, Thin Solid Films 284–285 (1996) 432–435.
[4] A. Tronin, J. Strzalka, X. Chen, P.L. Dutton, J.K. Blasie, Determination of the porphyrin orientation distribution in Langmuir monolayers by polarized epi-fluorescence, Langmuir 16 (2000) 9878–9886.
[5] H. Imahori, T. Hasobe, H. Yamada, Y. Nishimura, I. Yamazaki, S. Fukuzumi, Concentration effects of porphyrin monolayers on the structure and photoelectrochemical properties of mixed self-assembled monolayers of porphyrin and alkanethiol on gold electrodes, Langmuir 17 (2001) 4925–4931.
[6] D.-J. Qian, C. Nakamura, J. Miyake, Spectroscopic studies of the multiporphyrin arrays at the air–water interface and in Langmuir–Blodgett films, Thin Solid Films 397 (2001) 266–275.
[7] T.H. Richardson, C.M. Dooling, O. Worsfold, L.T. Jones, K. Kato, K. Shinbo, F. Kaneko, R. Treggoning, M.O. Vysotskyd, C.A. Hunter, Taking advantage of optical and electrical properties of organic molecules for gas sensing applications, Thin Solid Films 393 (2001) 259–266.
[8] L. Valkova, N. Borovkov, M. Pisani, F. Rustichelli, Structure of monolayers of copper tetra-(3-nitro-5-tert-butyl)-phthalocyanine at the air–water interface, Langmuir 17 (2001) 3639–3642.
[9] R. Paolesse, L. Valli, C. Goletti, C.D. Natale, A. Froiio, A. Macagnano, G. Bussetti, P. Chiaradia, A. D'Amico, Langmuir–Blodgett films of a modified tetraphenylporphyrin, Mater. Sci. Eng. C 22 (2002) 219–225.
[10] J.-R. Koo, H.-S. Lee, Y. Ha, Y.-H. Choi, Y.K. Kim, Electrical properties of porphyrin-based switching devices, Thin Solid Films 438–439 (2003) 123–127.
[11] A. Boguta, D. Wrobel, A. Bartczak, R. Swietlik, Z. Stachowiak, R.M. Ion, Characterization of interfacial effects in organic macrocycles Langmuir and Langmuir–Blodgett layers studied by surface potential and FT–IR spectroscopy examination, Mater. Sci. Eng. B 113 (2004) 99–105.
[12] Y. Zhou, B. Wang, M. Zhu, J.G. Hou, Observation of co-existence of 'face-on' and 'edge- on' stacking styles in a porphyrin monolayer, Chem. Phys. Lett. 403 (2005) 140–145.
[13] I. Capan, C. Tarimci, R. Capan, Fabrication of Langmuir–Blodgett thin films of porphyrins and investigation on their gas sensing properties, Sens. Actuators B 144 (2010) 126–130.
[14] Y.-H. Chan, A.E. Schuckman, L.M. Perez, M. Vinodu, C.M. Drain, J.D. Batteas, Synthesis and characterization of a thiol-tethered tripyridyl porphyrin on Au(1 1 1), J. Phys. Chem. C 112 (2008) 6110–6118.
[15] J.M. Pedrosa, C.M. Dooling, T.H. Richardson, R.K. Hyde, C.A. Hunter, M.T. Martin, L. Camacho, Influence of molecular organization of asymmetrically substituted porphyrins on their response to NO_2 gas, Langmuir 18 (2002) 7594–7601.
[16] L. Valkova, N. Borovkov, M. Pisani, F. Rustichelli, Three-dimensional structure of the copper porphyrazine layers at the air–water interface, Thin Solid Films 401 (2001) 267–272.
[17] H.-G. Liu, D.-J. Qian, X.-S. Feng, Q.-B. Xue, K.-Z. Yang, Monolayer studies on an acetic acid substituted porphyrin and its complexes with aliphatic amines or quaternary ammonium salts at the air–liquid interface, Langmuir 16 (2000) 5079–5085.
[18] B.W. Gregory, D. Vaknin, J.D. Gray, B.M. Ocko, T.M. Cotton, W.S. Struve, Two-dimensional crystallization of phthalocyanine pigments at the air/water interface, J. Phys. Chem. B 103 (1999) 502–508.
[19] A. Borodin, M. Kiselev, Structure of the porphyrazine monolayer at the air–water interface: computer simulation, Pure Appl. Chem. 76 (2004) 197–202.
[20] S. Krongsuk, T. Kerdcharoen, A. Borodin, M. Kiselev, Computer simulation study of a porphyrazine monolayer at a water–gas interface: structure and molecular orientation, J. Korean Phys. Soc. 52 (2008) 1657–1660.
[21] J. Rezac, J. Fanfrlik, D. Salahub, P. Hobza, Semiempirical quantum chemical PM6 method augmented by dispersion and H-bonding correction terms reliably describes various types of noncovalent complexes, J. Chem. Theory Comput. 5 (2009) 1749–1760.
[22] P.M. Kozlowski, M.Z. Zgierski, P. Pulay, An accurate in-plane force field for porphine. A scaled quantum mechanical study, Chem. Phys. Lett. 247 (1995) 379–385.
[23] D. Lamoen, M. Parrinello, Geometry and electronic structure of porphyrins and porphyrazines, Chem. Phys. Lett. 248 (1996) 309–315.
[24] E.J. Baerends, G. Ricciardi, A. Rosa, S.J.A.v. Gisbergen, A DFT/TDDFT interpretation of the ground and excited states of porphyrin and porphyrazine complexes, Coordin. Chem. Rev. 230 (2002) 5–27.
[25] O. Cramariuc, T.I. Hukka, T.T. Rantala, A DFT study of asymmetric meso-substituted porphyrins and their zinc complexes, Chem. Phys. 305 (2004) 13–26.
[26] A.D.F. Dunbar, T.H. Richardson, A.J. McNaughton, J. Hutchinson, C.A. Hunter, Investigation of free base, Mg, Sn, and Zn substituted porphyrin LB films as gas sensors for organic analytes, J. Phys. Chem. B 110 (2006) 16646–16651.
[27] C. Muck-Lichtenfeld, S. Grimme, Structure and binding energies of the porphine dimer, Mol. Phys. 105 (2007) 2793–2798.
[28] N.A. McDonald, W.L. Jorgensen, Development of an all-atom force field for heterocycles. Properties of liquid pyrrole, furan, diazoles, and oxazoles, J. Phys. Chem. B 102 (1998) 8049–8059.
[29] X.X. Zhang, N. Kobayashi, J.Z. Jiang, NMR spectra of free-base porphine, porphyrazine, phthalocyanine and naphthalocyanine as well as their metal complexes: density functional calculations, Spectrochim. Acta A 64 (2006) 526–531.
[30] H.J.C. Berendsen, J.P.M. Postma, W.F.V. Gunsteren, J. Hermans, in: B. Pullman (Ed.), Intermolecular forces, Dordrecht, Reidel, 1981.
[31] J.-P. Ryckaert, G. Ciccotti, H.J.C. Berendsen, Numerical integration of the cartesian equations of motion of a system with constraints: molecular dynamics of n-alkanes, J. Comp. Phys. 23 (1977) 327–341.
[32] H. Kuhn, H. Rehage, Molecular dynamics computer simulations of surfactant monolayers: monododecyl pentaethylene glycol at the surface between air and water, J. Phys. Chem. B 103 (1999) 8493–8501.
[33] H.J.C. Berendsen, J.P.M. Postma, W.F.v. Gunsteren, A. DiNola, J.R. Haak, Molecular dynamics with coupling to an external bath, J. Chem. Phys. 81 (1984) 3684–3690.
[34] U. Essmann, L. Perela, M.L. Berkowitz, T. Darden, H. Lee, L.G. Pedersen, A smooth particle mesh Ewald method, J. Chem. Phys. 103 (1995) 8577–8592.
[35] H.J.C. Berendsen, D.V.D. Spoel, R.V. Drunen, GROMACS: a message-passing parallel molecular dynamics implementation, Comp. Phys. Commun. 91 (1995) 43–56.
[36] E. Lindahl, B. Hess, D.V.D. Spoel, GROMACS 3.0: a package for molecular simulation and trajectory analysis, J. Mol. Mod. 7 (2001) 306–317.
[37] W. Humphrey, A. Dalke, K. Schulten, VMD—Visual molecular dynamics, J. Mol. Graphics 14 (1996) 33–38.
[38] C.A. Hunter, J.K.M. Sanders, The nature of π–π interactions, J. Am. Chem. Soc. 112 (1990) 5525–5534.

Please cite this article in press as: S. Krongsuk, T. Kerdcharoen, Effects of surface concentration on the porphine monolayers: Molecular simulations at the nanoscale water–gas interface, Appl. Surf. Sci. (2011), doi:10.1016/j.apsusc.2011.02.058

The Hydration Structure of Porphine in Aqueous Solution as Studied by Monte Carlo Simulation Based on Using Ab Initio Potential Models

Krongsuk, S.[1*], and Kerdcharoen, T.[2]

[1]*Department of Physics, Faculty of Science, Khon Kaen University, 123 Mittraparp Road, Khon Kaen 40002, Thailand*
[2]*Center of Intelligent Materials and Systems and Department of Physics, Faculty of Science, Mahidol University, Rama 6 Road, Bangkok 10400, Thailand*

Abstract

The hydration structure of porphine (PH_2) molecule has been investigated by using Monte Carlo simulation method. A simulation has been carried out for a system containing one porphine and 500 water molecules in a cubic box. With a volume of 500 water molecules at 298 K and 1 atm plus additional space occupied by the porphine molecule, a periodic cubic volume of side length of 25.0 Å was yielded. A potential model describing interaction between the porphine and water molecules has been newly developed based on *ab initio* calculations, while the MCY potential model was employed to represent water-water interaction. The simulation result showed that there five hydration layers around the porphine have been detected. The first and second layers were named the nearest-neighbor and inner hydration shells and the corresponding numbers of water molecules lying in such shells are 1 and 6, respectively. The water molecule in the nearest-neighbor shell showed two preferential orientations. One most probability orientation is that the water molecule points its dipole moment parallel to the ligand plane and the other one is that its dipole moment points away from the ligand center with the angle of 50° respect to the z-axis.

Keywords: Porphyrins, Porphine, Hydration, Ab initio potential, Monte Carlo simulation, Water orientation

*Corresponding author.
Tel.: 0-4320-3166; Fax: 0-4320-2374
E-mail: srikro@kku.ac.th

Molecular structures and dynamics of the porphine and porphine/Zn^{+2} complex monolayer films at the water-gas interface. A molecular dynamics study.

Sriprajak Krongsuk[1*], Teerakiat Kerdchareon[2]

[1]*Physics Department, Faculty of Science, Khon Kaen University, 123 Mittaparp Road, Khon Kaen 40002, Thailand*
[2]*Physics Department and Center of Nanoscience and Nanotechnology, Faculty of Science, Mahidol University, Rama 6 Road, Bangkok 10400, Thailand*

Abstract

Interfacial structure and orientation of the monolayer films of porphine (Ph2) and its complex with Zn^{+2} ion (ZnPh2) have been studied by using a molecular dynamic (MD) technique. The system model consists of 15 Ph2 and 15 ZnPh2 molecules regularly distributed on a water surface of 3.77x3.77 nm^2. Two monolayer systems have been simulated at the temperature of 300 K and the constant volume. The results revealed that density distributions of Ph2 and ZnPh2 are quite significant different. The density peak of ZnPh2 is narrower and sharper than that of Ph2. This means that the ZnPh2 molecules favorite to stay locally at the interface. In addition, it has been observed from the density of water in the interface region that there is a small peak appeared at the interface. This implies that the interaction between water and ZnPh2 molecules is stronger than the interaction between water and Ph2 molecules. Molecular orientations of Ph2 and ZnPh2 molecules on the water surface have been investigated by calculating the distribution of molecular tilted angle. The results shown that the Ph2 molecules prefer to tilt with the angle of 66.4° respect to the interface plane, while the tilted angles of ZnPh2 molecules is 71.0° and 90°, respectively. The tilted angles of 66.4° to 71.0° are assumed to correspond to the α-form of crystalline phthalocyanine which is the most stable form.

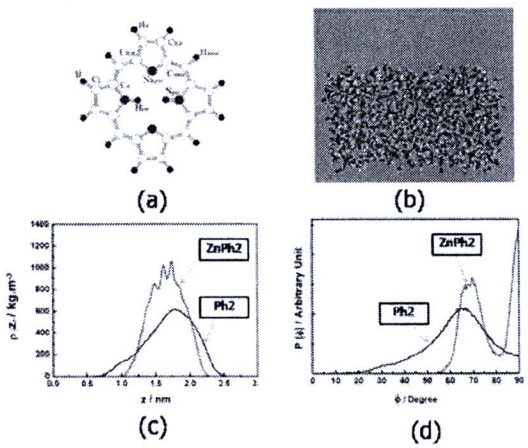

Fig. 1 (a) Porphine structure,
(b) Monolayer of porphine on the water surface
(c) Density distributions of Ph2 and ZnPh2 molecules
(d) Tilted angle distributions of Ph2 and ZnPh2 molecules

Keywords: Porphine monolayer, density profile, tilted angle, molecular dynamics

*Corresponding author.
Tel.: +66-4320-3166; Fax: +66-4320-2374
E-mail: srikro@kku.ac.th